Rayleigh-Bénard problem with imposed weak through-flow: Two coupled Ginzburg-Landau equations

H. W. Müller
Department of Physics and Center for Nonlinear Sciences, University of California, Santa Barbara, Santa Barbara, California 93106; Institut für Theoretische Physik, Universität des Saarlandes, D-6600 Saarbrücken, Germany; and Laboratoire de Physique, Ecole Normale Supérieure de Lyon, 46 Allée d'Italie, 69364 Lyon, France

M. Tveitereid
Department of Physics and Center for Nonlinear Sciences, University of California, Santa Barbara, Santa Barbara, California 93106 and Adger College of Engineering, N-4890 Grimstad, Norway

S. Trainoff
Department of Physics and Center for Nonlinear Sciences, University of California, Santa Barbara, Santa Barbara, California 93106
(Received 23 June 1992; revised manuscript received 4 February 1993)

The Rayleigh-Bénard instability of a horizontal shear flow in a narrow channel is governed by two competing unstable modes: traveling transverse and stationary longitudinal convection rolls. The dynamics of the mode amplitudes obeys two coupled Ginzburg-Landau equations, which we derive in the present article. For mathematical simplicity we assume free-slip boundaries at the channel sidewalls. The analytical discussion and the numerical simulation of these amplitude equations show transitions between the two convective structures. Propagating fronts, which separate areas of transverse rolls and longitudinal ones, occur in the parameter range where both patterns are stable. Coexisting uniform states with nonzero amplitudes of both modes are unstable solutions of the equations. Results are in qualitative agreement with recent experiments.

PACS number(s): 47.20.Bp, 47.20.Ky, 47.60.+i

I. INTRODUCTION

The purpose of this paper is to investigate the nonlinear dynamics of fluid flowing down in a long narrow channel heated from below. Historically, this problem was motivated by the observation of cloud streets in the earth's atmosphere [1]. Here, cold air (wind) is heated by the ground and forms convection rolls oriented parallel to the prevailing wind direction. The convection is visualized when the warm air cools and the water vapor it contains condenses into clouds along the up-flow boundaries. However, the present interest in this phenomenon transcends the original historical context and concentrates on the more general problem of pattern formation in nonlinear systems. It turns out that the thermogravitational instability of a horizontal fluid layer [Rayleigh-Bénard convection (RBC)] combined with the stability problem of a laminar shear flow (Orr-Sommerfeld problem) leads to interesting bifurcation behavior [2]. This is due to the interplay of transport and instability arising from the *convective* nature of the primary bifurcation and the *absolute* instability at higher Rayleigh numbers [3].

Experimentally, RBC can be precisely controlled and measured in the laboratory. Depending on the width of the channel and the through-flow rate one observes either traveling convection rolls with axes perpendicular to the flow [transverse rolls (TR)] or stationary rolls with axes aligned in the streamwise direction [longitudinal rolls (LR)]. Most experimental work deals with either of these structures [4–7]. Only recently, experimental investigations of the transition between TR and LR showed coexistence and/or time-dependent states [8,9].

The linear stability of the problem is well known. In a fluid layer without lateral boundaries, it has been shown [10, 11] that the onset of convection always occurs in the form of stationary LR. When the influence of sidewalls is taken into account [12], the preferred pattern in a narrow channel with a weak shear flow consists of traveling TR. With stronger flows, the effect of the walls is overcome and the rolls switch their axes to again align with the flow. Brand, Deissler, and Ahlers [13] have studied this nonlinear problem by examining a phenomenological model of two coupled envelope equations for LR and TR. Several of their findings are in qualitative agreement with the experimental observations [8,9].

In this article we derive the envelope equations systematically from the basic hydrodynamic field equations. Following the work of Müller, Lücke, and Kamps [14], who determined the amplitude equation for TR, we calculate the corresponding equation for the LR mode and the nonlinear coupling terms that govern the competition between the two states. It turns out that the equations are of a different structure than assumed by Brand, Deissler, and Ahlers [13]. An important objective of this publication is to present the derivation of these amplitude equations and to provide numerical values for their coefficients. We discuss the nonlinear solutions analytically and investigate their stability. Finally we present numerical simulations which have relevance to the stability analysis and the experimental findings.

 ©1993 The American Physical Society

II. GOVERNING EQUATIONS

We consider a viscous incompressible fluid layer of thickness h confined between two rigid perfectly heat conducting horizontal planes. To describe the geometry we use Cartesian coordinates (x,y,z) with unit vectors $\mathbf{e}_x$, $\mathbf{e}_y$, $\mathbf{e}_z$. The origin is located at the lower boundary and the z axis is directed vertically upwards. We shall examine the flow which is generated by a constant temperature difference ΔT between the planes and by an applied constant pressure gradient β in the negative x direction. The coordinates, time, velocity, pressure, and temperature are made dimensionless by scaling with h, h^2/κ, κ/h, $\rho_0\kappa\nu/h^2$, and ΔT, respectively, where κ is the thermal diffusivity, ν the kinematic viscosity, and ρ_0 a reference density.

By using the Boussinesq approximation, the Navier Stokes, continuity, and heat equations admit a time-independent solution with velocity $\mathbf{U}$ (plane Poiseuille flow), pressure gradient ∇P, and temperature gradient ∇T according to

$$\mathbf{U}=\sigma\,\mathrm{Re}U(z)\mathbf{e}_x\ ,\quad U(z)=6(1-z)z\ , \tag{2.1a}$$

$$\nabla P=-12\sigma\,\mathrm{Re}\mathbf{e}_x-\frac{\mathrm{Ra}}{\gamma\Delta T}(1+\gamma\Delta Tz)\mathbf{e}_z\ , \tag{2.1b}$$

$$\nabla T=-\mathbf{e}_z\ . \tag{2.1c}$$

Here σ is the Prandtl number, Re the Reynolds number, and Ra the Rayleigh number defined by

$$\sigma=\kappa/\nu\ ,\quad \mathrm{Re}=U_m h/\nu\ ,\quad \mathrm{Ra}=\gamma g h^3\Delta T/(\kappa\nu)\ , \tag{2.2}$$

where $U_m=\beta h^2/(12\rho_0\nu)$ is the averaged velocity of the Poiseuille flow, γ is the coefficient of thermal expansion, and g is the acceleration of gravity. Note that (2.1) becomes the familiar conduction state in RBC as $\mathrm{Re}\to 0$.

To investigate the problem when the base flow solution (2.1) is unstable, we superimpose perturbations of velocity $\mathbf{v}=(u,v,w)$, pressure p, and temperature θ and obtain from the hydrodynamic equations:

$$\frac{1}{\sigma}(\partial_t+\mathbf{v}\cdot\nabla)\mathbf{v}+\mathrm{Re}(U\partial_x\mathbf{v}+(\partial_z U)w\mathbf{e}_x)$$
$$=-\nabla p+\mathrm{Ra}\theta\mathbf{e}_z+\nabla^2\mathbf{v}\ , \tag{2.3a}$$

$$(\partial_t+\mathbf{v}\cdot\nabla)\theta+\sigma\,\mathrm{Re}U\partial_x\theta-w=\nabla^2\theta\ , \tag{2.3b}$$

$$\nabla\cdot\mathbf{v}=0\ , \tag{2.3c}$$

with the realistic no-slip boundary conditions at the top and bottom

$$u=v=w=\theta=0\quad\text{at } z=0,1\ . \tag{2.4}$$

There are two instability mechanisms of the base flow (2.1), giving a nonzero solution of Eqs. (2.3). One is the so-called Tollmien-Schlichting instability [15], which occurs for large values of Re and $\mathrm{Ra}<1708$. The second type is the Rayleigh-Bénard instability [16] for values of Ra larger than 1708. In this paper we consider the latter case and discuss weakly nonlinear solutions for small through-flow rates.

III. LINEAR STABILITY ANALYSIS

The linear stability analysis of the basic state (2.1) has been carried out [10,11] for a fluid layer of infinite lateral extension by considering linear solutions of Eqs. (2.3) of the form

$$[\mathbf{v},p,\theta]=[\hat{\mathbf{v}}(z),\hat{p}(z),\hat{\theta}(z)]e^{i(kx+ly-\omega t)}\ . \tag{3.1}$$

Here $\hat{\mathbf{v}},\hat{p},\hat{\theta}$ are z-dependent eigenfunctions, ω is the frequency, and $\mathbf{q}=(k,l)$ is the wave vector with components k and l in the x and y directions, respectively. The onset of instability is determined by imposing ω to be real. If a solution in form of TR, i.e., $\mathbf{q}=(k,0)$, is considered, the roll axes are orthogonal to $\mathbf{U}$ and the neutral values for Ra and ω are functions of k, Re, and σ. For given values of Re and σ the minimum value Ra_c^T of Ra occurs at wave number k_c and frequency ω_c^T. For $\sigma=5.8$ and Re up to unity we have fitted these values to polynomials in Re and found

$$\mathrm{Ra}_c^T=\mathrm{Ra}_{c0}+\mathrm{Ra}_{c2}\mathrm{Re}^2+O(\mathrm{Re}^4)\ , \tag{3.2a}$$

$$k_c=k_{c0}+k_{c2}\mathrm{Re}^2+O(\mathrm{Re}^4)\ , \tag{3.2b}$$

$$\omega_c^T=\omega_{c1}\mathrm{Re}+\omega_{c3}\mathrm{Re}^3+O(\mathrm{Re}^5)\ . \tag{3.2c}$$

Here Ra_{c0} and k_{c0} are the critical values known from the Rayleigh-Bénard problem [16]. The values of the expansion coefficients Ra_{c2}, k_{c2}, ω_{c1}, and ω_{c3} are listed in Table I.

By use of Squire's theorem [10,11,17] one obtains from the expansions (3.2) the critical values for any other lateral wave vector $\mathbf{q}$ by substituting q_c for k_c and $(k/q)\mathrm{Re}$ for Re, where $q=(k^2+l^2)^{1/2}$. For a LR pattern, i.e., $k=0$ the onset of instability is stationary and independent of Re, and one finds

$$\mathrm{Ra}_c^L=\mathrm{Ra}_{c0}\ ,\quad l_c=k_{c0}\ ,\quad \omega_c^L=0\ . \tag{3.3}$$

The critical Rayleigh number for oblique rolls attains a value between Ra_c^T and Ra_c^L, depending on the orientation of the roll axes in the horizontal plane.

Figure 1 gives a schematic sketch of the critical values of Ra for TR and LR as functions of the Reynolds number. For convention we have introduced the reduced Rayleigh number ϵ, defined by

$$\epsilon=\mathrm{Ra}/\mathrm{Ra}_{c0}-1\ . \tag{3.4}$$

The solid lines indicate the stability boundaries for a fluid layer of infinite lateral extension. The dashed lines denote the corresponding thresholds if the fluid is confined between sidewalls parallel to the Poiseuille flow. It has been shown theoretically [12] and experimentally [8,12] that sidewalls stabilize the basic state (2.1): the critical values of Ra increase with decreasing distance be-

TABLE I. Values of the expansion coefficients for the critical stability quantities Ra_c^T, k_c, and ω_c^T in (3.2) for a Prandtl number of $\sigma=5.8$.

$\mathrm{Ra}_{c0}=1707.762$	$\mathrm{Ra}_{c2}=15.5528$
$k_{c0}=3.116$	$k_{c2}=-0.006\,95$
$\omega_{c1}=23.1709$	$\omega_{c3}=-0.046\,47$

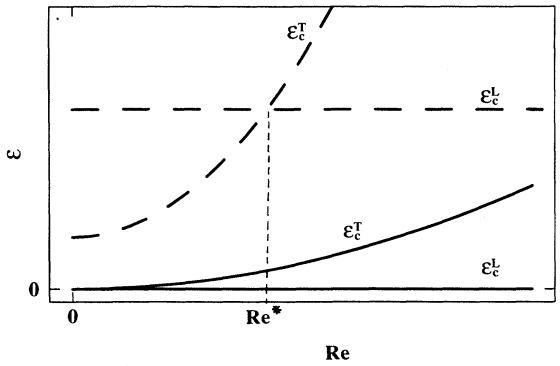

FIG. 1. Sketch of the linear stability boundaries for a fluid layer without (solid) and with (dashed) lateral sidewalls. The conductive state (2.1) is unstable with respect to traveling transverse rolls (TR) at $\epsilon > \epsilon_c^T$ and unstable to stationary longitudinal rolls (LR) at $\epsilon > \epsilon_c^L$. Re* denotes the codimension two point. The stabilization of the conductive state due to sidewalls depends on the distance between them.

tween the sidewalls. An interesting feature at small values of Re is that the stabilization is more effective for LR than for TR. This gives that ϵ_c^T and ϵ_c^L intersect at a nonzero value of Re, which we identify as Re*. Close to this codimension two point the dynamics of the competing traveling TR and stationary LR leads to interesting convection behavior.

IV. WEAKLY NONLINEAR THEORY

In this section we derive the coupled nonlinear amplitude equations for TR and LR. Our objective is to provide a theoretical model for the competitive dynamics between the two flow patterns in a narrow infinite long channel. Due to the presence of the sidewalls a rigorous treatment of the problem requires a numerical analysis in *two* spatial dimensions (y and z), e.g., by a two-dimensional Galerkin method. However, to keep the mathematics as simple as possible we consider free-slip boundary conditions at the sidewalls and impose the distance in between to be a small integral multiple of $2\pi/l_c$ (equal to critical wavelength for a fluid layer without lateral boundaries). The mathematical model therefore is defined by Eqs. (2.3) and (2.4). In order to incorporate the stabilizing influence of the sidewalls we do not use the stability curves $\epsilon_c^T(\mathrm{Re})$ and ϵ_c^L for a fluid of infinite lateral extension since they intersect at $\mathrm{Re}^*=0$. Instead, we take *ad hoc* values giving a codimension two point at $\mathrm{Re}^* > 0$ (c.f. Fig. 1). Additional sidewall effects (e.g., deformation of the eigenfunctions in narrow channels) are ignored.

We shorten the notation by casting Eqs. (2.3) into the form

$$\underline{L}\varphi = N(\varphi,\varphi) \ . \tag{4.1}$$

Here $\underline{L}$ is a linear 8×8 matrix operator defined in the Appendix, and the eight-dimensional vectors

$$\varphi = (u,v,w,\theta,\partial_z u,\partial_z v,p,\partial_z\theta)^t \ , \tag{4.2a}$$

$$N(\varphi,\varphi) = \frac{1}{\sigma}(\mathbf{v}\cdot\nabla)(0,0,0,0,u,v,-w,\sigma\theta)^t \ , \tag{4.2b}$$

represent the solution and the quadratic nonlinearity. The superscript t denotes the transpose.

From the nonlinear solution of the Rayleigh-Bénard problem it is known [18] that the convective amplitude is of $O(\delta)$ when $\epsilon-\epsilon_c = O(\delta^2)$. Moreover, from the form of the neutral curve in the (q,ϵ) plane it follows that those disturbances are excited whose wave numbers q are lying within a band of $O(\delta)$ around the critical value q_c. The bandwidths Δk and Δl in the x and, respectively, the y direction depend on the geometry of the channel and the orientation of the roll pattern under consideration. In a narrow infinitely long channel, with the y axis parallel to the short side, slow variations in y directions do not appear so that $\Delta l = 0$ is enforced. The value of Δk is given by the restriction $q = q_c + O(\delta)$. Here, one finds $\Delta k = O(\delta)$ for a pattern of TR and $\Delta k = O(\delta^{1/2})$ for a pattern of LR. The interaction of the modes within these wave-number bands leads to slow spatial and temporal variations of the nonlinear convection. In order to accommodate these variations the amplitudes are taken to be slowly varying functions [19,20] of x and t. We therefore adopt the method of multiple scales [21] by defining

$$\partial_t \leftarrow \partial_t + \delta^{1/2}\partial_{T1/2} + \delta\partial_{T1} + \delta^{3/2}\partial_{T3/2} + \cdots \ , \tag{4.3a}$$

$$\partial_x \leftarrow \partial_x + \delta^{1/2}\partial_{X1/2} + \delta\partial_{X1} + \delta^{3/2}\partial_{X3/2} + \cdots \ . \tag{4.3b}$$

For small supercritical values of ϵ we are led to seek solutions of Eq. (4.1) by the expansion

$$\varphi = \delta\varphi_1 + \delta^{3/2}\varphi_{3/2} + \delta^2\varphi_2 + \cdots \ . \tag{4.4}$$

By using (4.3) and (4.4) we also expand $\underline{L}$ and N in powers of δ as

$$\underline{L} = \underline{L}_0 + \delta^{1/2}\underline{L}_{1/2} + \delta\underline{L}_1 + \cdots \ , \tag{4.5a}$$

$$N = \delta^2 N_2 + \delta^{5/2}N_{5/2} + \delta^3 N_3 \ldots \ . \tag{4.5b}$$

The matrix $\underline{L}_0$ follows from $\underline{L}$ simply by taking Ra at its critical value; the full effect of the Rayleigh number is reobtained in $\underline{L}_2$. The matrices $\underline{L}_i$ and the vectors N_i are defined in the Appendix. By introducing the expansions for $\underline{L}$, φ, and N into Eq. (4.1) the following hierarchic set of linear equations [up to $O(\delta^3)$] is obtained:

$$\underline{L}_0\varphi_1 = 0 \quad [O(\delta)] \ , \tag{4.6a}$$

$$\underline{L}_0\varphi_{3/2} = -\underline{L}_{1/2}\varphi_1 \quad [O(\delta^{3/2})] \ , \tag{4.6b}$$

$$\underline{L}_0\varphi_2 = -\underline{L}_{1/2}\varphi_{3/2} - \underline{L}_1\varphi_1 + N_2 \quad [O(\delta^2)] \ , \tag{4.6c}$$

$$\underline{L}_0\varphi_{5/2} = -L_{1/2}\varphi_2 - \underline{L}_1\varphi_{3/2} - \underline{L}_{3/2}\varphi_1 + N_{5/2} \quad [O(\delta^{5/2})] \ , \tag{4.6d}$$

$$\underline{L}_0\varphi_3 = -L_{1/2}\varphi_{5/2} - \underline{L}_1\varphi_2 - \underline{L}_{3/2}\varphi_{3/2} - \underline{L}_2\varphi_1 + N_3 \quad [O(\delta^3)] \ . \tag{4.6e}$$

Any solution vector φ_j has to fulfill the boundary conditions (2.4), giving

$$\varphi_j^{(1)} = \varphi_j^{(2)} = \varphi_j^{(3)} = \varphi_j^{(4)} = 0 \quad \text{at } z = 0 \ , 1 \ , \tag{4.7}$$

where $\varphi_j^{(i)}$ denotes the ith component of the vector φ_j.

The leading-order Eq. (4.6a) defines the linear stability problem, and we consider a solution composed of downstream traveling TR and stationary LR:

$$\varphi_1 = A\hat{\varphi}_A(z)e^{i(kx-\omega t)} + B\hat{\varphi}_B(z)e^{ily} + \text{c.c.} \tag{4.8}$$

A set of TR propagating in the counterflow direction does not appear since the spatial $x \to -x$ symmetry is broken by the through flow.

Due to the different bandwidths Δk for TR and LR the amplitudes A and B are supposed to depend on the slow time and space coordinates $(X_1, T_1, X_2, T_2, \ldots)$ and $(X_{1/2}, T_{1/2}, X_1, T_1, \ldots)$, respectively. To shorten notation we write k, l, ω instead of the critical quantities k_c, l_c, ω_c^T. The two eigensolutions $\hat{\varphi}_A(z)$ and $\hat{\varphi}_B(z)$ are generated numerically (using a shooting scheme) by solving the stability problem (4.6a) separately for TR and for LR (with $\mathrm{Ra}=\mathrm{Ra}_c^T$ and, respectively, $\mathrm{Ra}=\mathrm{Ra}_c^L$ in $\underline{L}_0$). Consequently, the natural expansion parameter is $\epsilon-\epsilon_c^T$ for transverse rolls and $\epsilon-\epsilon_c^L$ for longitudinal rolls. To organize the expansion procedure consistently, and to match the cross coupling between TR and LR in $O(\delta^3)$, we assume

$$O(\epsilon-\epsilon_c^T) = O(\epsilon-\epsilon_c^L) = O(\delta^2) . \tag{4.9}$$

This implies $O(\epsilon_c^T-\epsilon_c^L)=O(\delta^2)$, meaning that any nonlinear solution giving coupling between TR and LR is valid in a δ^2 neighborhood of the codimension two point Re^*, where ϵ_c^T and ϵ_c^L intersect.

On solving system (4.6) iteratively, we find that the slowly varying amplitudes are governed by the following Ginzburg-Landau equations:

$$\begin{aligned}\tau_A(\partial_t + v_A\partial_x)A = [&(\epsilon-\epsilon_c^T)(1+ic_0) + \xi_A^2(1+ic_1)\partial_x^2 \\ &-(1+ic_2)|A|^2 \\ &-\beta_A(1+ic_3)|B|^2]A ,\end{aligned} \tag{4.10a}$$

$$\begin{aligned}\tau_B(\partial_t + v_B\partial_x)B = [&(\epsilon-\epsilon_c^L) + \xi_B^2\partial_x^2 + \chi_B\partial_x^3 - \lambda_B\partial_x^4 \\ &-|B|^2 - \beta_B|A|^2]B .\end{aligned} \tag{4.10b}$$

Table II presents fit formulas of the coefficients for Re up to unity and $\sigma=5.8$. The coefficients appearing on the right-hand side of (4.10a) are complex because the TR instability of the basic conductive state is oscillatory. Apart from the nonlinear coupling term $|B|^2A$ this equation has previously been derived by Müller, Lücke, and Kamps [14].

TABLE II. List of the linear and nonlinear coefficients of the amplitude equations (4.10) for a Prandtl number of $\sigma=5.8$.

$\tau_A = 0.0554 + 0.000\,07\,\mathrm{Re}^2$	$c_0 = 0.0187\,\mathrm{Re}$
$v_A = 7.507\,\mathrm{Re}$	$c_1 = 0.0382\,\mathrm{Re}$
$\xi_A^2 = 0.1482 + 0.001\,16\,\mathrm{Re}^2$	$c_2 = -0.0030\,\mathrm{Re}$
$\beta_A = 1.2486 + 0.0025\,\mathrm{Re}^2$	$c_3 = -0.0450\,\mathrm{Re}$
$\tau_B = 0.0554 - 2.7\ 10^{-8}\,\mathrm{Re}^2$	$v_B = 7.435\,\mathrm{Re}$
$\xi_B^2 = 0.0010\,\mathrm{Re}^2$	$\chi_B = 0.000\,21\,\mathrm{Re}$
$\beta_B = 1.2486 + 0.0012\,\mathrm{Re}^2$	$\lambda_B = 0.0038 + 0.000\,01\,\mathrm{Re}^2$

The amplitude equation for B is new; it possesses pure real coefficients. This is a general consequence of the stationary LR instability and the reflection symmetry of the system at the midplane between the sidewalls. Indeed, the transformation $y \to -y$ in (4.8) forces the evolution equation (4.10b) to be invariant under $B \to B^*$. In the absence of through flow ($\mathrm{Re}=0$) the lowest-order nonvanishing gradient term $\partial_x^4 B$ dominates the spatial dependence of B. As soon as the flow is turned on the anisotropy in the x direction creates a first-, a second-, and a third-order space derivative. It can be seen from Table II that the correction due to the ∂_x^3 term is always negligible in comparison to the advective term $v_B\partial_x B$ (at least in the range of validity of the envelope equations, where $\Delta k \ll k_c$). By virtue of the $[x \to -x,\ \mathrm{Re} \to -\mathrm{Re}]$ symmetry the second-order coefficient ξ_B^2 increases proportional to the square of Re. For a typical flow rate of $\mathrm{Re} \simeq 0.5$ it follows from Table II that the modulational dynamics on spatial scales slower than $\Delta k \simeq 0.25$ is already governed by the second-order derivative. This has been pointed out by Brand, Deissler, and Ahlers [13]; however, in their model they ignored the Re dependence of ξ_B^2 and assumed a numerical value being two orders of magnitude higher.

On the other hand, when we solve Eqs. (4.10) numerically (Sec. VI), the derivative terms become large in the inlet and outlet regions of the channel, or in the transition zones between TR and LR. This corresponds to modulational wave numbers with large imaginary parts. Likewise, when examining the boundary of absolute instability (Sec. V), the fourth-order derivative term in (4.10b) dominates the second derivative for $\mathrm{Re} \cong 1$. We therefore include all terms of Eq. (4.10) in the following discussion.

The most important difference between the envelope equations (4.10) and the phenomenological model of Ref. [13] concerns the nonlinear coupling coefficients β_A and β_B. These are substantial for the predicted pattern competition (see below). According to Table II the values of β_A and β_B weakly depend on Re so that they are well approximated by the $\mathrm{Re}=0$ expression. Due to the rotational symmetry in the lateral plane the identity $\beta_A=\beta_B$ must hold in the absence of through flow. In addition, the appearance of rolls instead of squares [22] in RBC implies that $\beta_A=\beta_B>1$. These arguments have not been addressed by Brand, Deissler, and Ahlers [13], who assumed the values $\beta_A=0.75$ and $\beta_B=1.5$ to achieve results compared with the experiments [7,9].

V. ANALYTICAL SOLUTIONS AND THEIR STABILITY

A. Absolute versus convective instability of the conductive state

The critical stability boundaries ϵ_c^T and ϵ_c^L mark the thresholds above which the basic conductive state $A \equiv 0 \equiv B$ becomes *convectively unstable* to perturbations in the form of TR and LR, respectively. Any *localized* initial disturbance is amplified in a comoving frame of reference but dies out at a *fixed* location. Convective

rolls therefore cannot grow globally and the system returns to the basic state. By virtue of the through flow the *absolute* instability thresholds $\epsilon^T_{\rm abs}$ and $\epsilon^L_{\rm abs}$ for which small localized perturbations are growing at *any* position, is shifted to higher values of ϵ. In the context of Ginzburg-Landau equations this problem has first been discussed by Deissler [23]. Upon solving the linearized amplitude equation (4.10a) for an initial pulse $\delta(x)$ (Dirac's δ function) the responding TR amplitude is found to be

$$A(x,t)\propto\frac{1}{t^{1/2}}\exp\left\{\frac{(\epsilon-\epsilon_c^T)(1+ic_0)t}{\xi_A^2}-\frac{(x-v_A\tau_A t/\xi_A^2)^2}{4(1+ic_1)t}\right\}. \tag{5.1}$$

This solution is exponentially growing for

$$4\frac{(\epsilon-\epsilon_c^T)(1+c_1^2)}{\xi_A^2}-\left[\frac{x}{t}-\frac{v_A\tau_A}{\xi_A^2}\right]^2>0\ . \tag{5.2}$$

By letting x fixed and $t\to\infty$ it follows that the basic state becomes absolutely unstable if

$$\epsilon>\epsilon^T_{\rm abs}\equiv\epsilon_c^T+\frac{(v_A\tau_A)^2}{4(1+c_1^2)\xi_A^2}\ , \tag{5.3}$$

and convectively unstable for $\epsilon_c^T<\epsilon<\epsilon^T_{\rm abs}$.

We then pose the same initial value problem for the linearized version of the LR equation (4.10b). Using the method of steepest descent one finds the asymptotic solution for x fixed and $t\to\infty$ as [24]

$$B(x,t)\propto\frac{1}{t^{1/2}}\exp\left\{\frac{(\epsilon-\epsilon_c^L)}{\lambda_B}t-\frac{3}{8\lambda_B}\left[\frac{v_B^4\tau_B^4}{4\lambda_B}\right]^{1/3}t\right\}. \tag{5.4}$$

Thus perturbations in the form of LR become absolutely unstable if

$$\epsilon>\epsilon^L_{\rm abs}\equiv\epsilon_c^L+\tfrac{3}{8}\left[\frac{v_B^4\tau_B^4}{4\lambda_B}\right]^{1/3}, \tag{5.5}$$

and convectively unstable for $\epsilon_c^L<\epsilon<\epsilon^L_{\rm abs}$.

Figure 2 shows the bifurcation boundaries $\epsilon_c^{T,L}$ and $\epsilon^{T,L}_{\rm abs}$ for the onset of convective and absolute instability. These lines are important to understand the numerics dis-

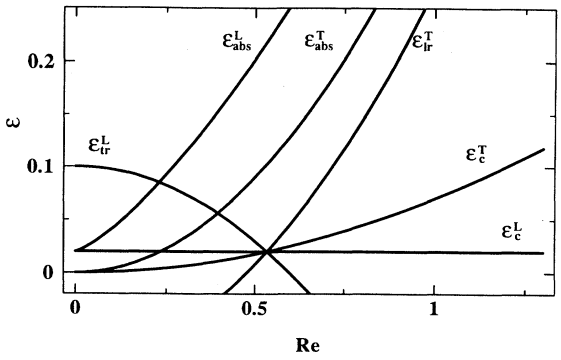

FIG. 2. Stability curves in the ϵ-Re control parameter plane: For $\epsilon_c^{T,L}<\epsilon<\epsilon^{T,L}_{\rm abs}$ ($\epsilon^{T,L}_{\rm abs}<\epsilon$) the basic conductive state (2.1) becomes convectively (absolutely) unstable to perturbations in the form of traveling TR or stationary LR, respectively. For $\epsilon<\epsilon^T_{\rm LR}$ ($\epsilon<\epsilon^L_{\rm TR}$) the uniform traveling TR state (stationary LR state) becomes unstable to perturbations in form of LR (TR) (see Sec. V for details). The values $\epsilon_c^T=0.07\,{\rm Re}^2$ and $\epsilon_c^L=0.02$ have been taken to obtain a codimension two point at ${\rm Re}^*\cong 0.5$.

cussed in Sec. VI. In the convectively unstable region any *initial* perturbation is carried away by the through flow so that a *continuous* source of perturbations is required to sustain permanent convection [23,25]. To take into account the effect of the sidewalls, which stabilize TR at small Re, we have taken $\epsilon_c^T=0.07\,{\rm Re}^2$ and $\epsilon_c^L=0.02$. These *ad hoc* values give a codimension two point at ${\rm Re}^*\cong 0.5$ as in the experiments of Ouazzani, Platten, and Mojtabi [8].

B. Stability of nonlinear solutions

Here we discuss uniform nonlinear solutions A_s and B_s of the coupled Ginzburg-Landau equations (4.10) of the form

$$A_s=A_0e^{i\Omega_A t}\ ,\quad B_s=B_0\ , \tag{5.6}$$

where A_0, B_0, and Ω_A are constants. To examine their stability we introduce space- and time-dependent perturbations $a(x,t)$, $b(x,t)$, and substitute $A=A_s+a$ and $B=B_s+b$ into (4.10). Subtracting the equations for the uniform solutions and linearizing in a and b gives the perturbation equations:

$$\tau_A(\partial_t+v_A\partial_x)a=[(\epsilon-\epsilon_c^T)(1+ic_0)+\xi_A^2(1+ic_1)\partial_x^2]a-(1+ic_2)(2|A_s|^2a+A_s^2a^*)$$
$$-\beta_A(1+ic_3)(|B_s|^2a+A_sB_s^*b+A_sB_sb^*)\ , \tag{5.7a}$$

$$\tau_B(\partial_t+v_B\partial_x)b=[(\epsilon-\epsilon_c^L)+\xi_B^2\partial_x^2+\chi_B\partial_x^3-\lambda_B\partial_x^4]b-(2|B_s|^2b+B_s^2b^*)-\beta_B(|A_s|^2b+A_s^*B_sa+A_sB_sa^*)\ , \tag{5.7b}$$

These equations possess separable solutions of the form

$$a=e^{\sigma_r t}(a_1e^{i(\alpha x+\sigma_i t)}+a_2e^{-i(\alpha x+\sigma_i t)})e^{i\Omega_A t}\ ,$$
$$b=e^{\sigma_r t}(b_1e^{i(\alpha x+\sigma_i t)}+b_2e^{-i(\alpha x+\sigma_i t)})\ , \tag{5.8}$$

and result in a quartic characteristic equation for the complex eigenvalues $\sigma=\sigma_r+i\sigma_i$. We define a given solution A_s, B_s as stable if all four values of σ_r are nonpositive for any real wave number α. The perturbations (5.8) represent a general stability analysis of the solution

(5.6) going beyond the investigation of Ref. [13], where pure real amplitude equations and space-independent disturbances ($\alpha=0$) have been considered. By inserting (5.6) into (4.10) we immediately find three different solutions: pure TR, pure LR, and coexistence of TR and LR (also called "mixed" states in Ref. [13]), which will be discussed by turns below.

1. TR pattern

Convection in the form of traveling TR is given by

$$|A_0|^2=\epsilon-\epsilon_c^T\ ,\quad \tau_A\Omega_A=(c_0-c_2)|A_0|^2\ ,\quad |B_0|^2=0\ . \tag{5.9}$$

This solution corresponds to a perfectly periodic TR pattern with wave number k_c and frequency $(\omega_c-\Omega_A)$. Note that Ω_A represents a nonlinear frequency correction.

The characteristic equation, which determines the stability of TR, separates into two quadratic equations for a and b. It turns out that a always is damped, whereas b is exponentially amplified if

$$\tau_B\sigma_r=\epsilon-\epsilon_c^L-\alpha^2\xi_B^2-\alpha^4\lambda_B-\beta_B|A_0|^2>0\ . \tag{5.10}$$

Since the fastest growing perturbation appears at $\alpha=0$ the TR pattern becomes unstable to LR perturbations by a long-wavelength instability at

$$\epsilon<\epsilon_{\rm LR}^T\equiv\epsilon_c^T+(\epsilon_c^T-\epsilon_c^L)/(\beta_B-1)\ . \tag{5.11}$$

This stability analysis has demonstrated that the uniform TR solution (5.9) is stable in a region of the (ϵ,Re) plane where $\epsilon\geq\max\{\epsilon_c^T,\epsilon_{\rm LR}^T\}$ (see Fig. 2). Here $\max\{\epsilon_c^T,\epsilon_{\rm LR}^T\}$ denotes the largest value of ϵ_c^T and $\epsilon_{\rm LR}^T$. The numerics in the next section will prove that the boundary ϵ_{LR}^T is indeed responsible for nonlinear transitions between TR and LR in the region $\mathrm{Re}>\mathrm{Re}^*$.

2. LR pattern

The solution

$$|A_0|^2=0\ ,\quad \Omega_A=0\ ,\quad |B_0|^2=\epsilon-\epsilon_c^L \tag{5.12}$$

corresponds to a stationary LR pattern with wave number l_c. Also for this solution the characteristic equation of the stability problem separates, giving always a negative growth rate for b. However, the temporal growth exponent of the TR perturbation a becomes positive for

$$\tau_A\sigma_r=\epsilon-\epsilon_c^T-\alpha^2\xi_A^2-\beta_A|B_0|^2\ . \tag{5.13}$$

As before, the fastest growing perturbation has $\alpha=0$, so that the LR pattern becomes unstable to TR perturbations if

$$\epsilon<\epsilon_{\rm TR}^L\equiv\epsilon_c^L+(\epsilon_c^L-\epsilon_c^T)/(\beta_A-1)\ . \tag{5.14}$$

The stable region of the uniform LR solution, given by $\epsilon\geq\max\{\epsilon_c^L,\epsilon_{\rm TR}^L\}$, is shown in Fig. 2. The following numerical section will confirm that a nonlinear transition from LR to TR appears at $\epsilon_{\rm TR}^L$ if $\mathrm{Re}<\mathrm{Re}^*$.

We mention that our $\epsilon_{\rm LR}^T$ coincides formally with the expression ϵ_7 of Brand, Deissler, and Ahlers [13] and our $\epsilon_{\rm TR}^L$ coincides with their ϵ_5. However, due to the different choice of the nonlinear coupling coefficients β_A and β_B the curve of ϵ_5 happens to appear close to our $\epsilon_{\rm LR}^T$ and the threshold ϵ_7 does not play a role in the stability diagram of Ref. [13].

3. Coexisting TR-LR pattern

When both amplitudes A_0 and B_0 are nonzero, the corresponding uniform solution

$$\begin{aligned}&(\beta_A\beta_B-1)|A_0|^2=\beta_A(\epsilon-\epsilon_c^L)-(\epsilon-\epsilon_c^T)\ ,\\ &(\beta_A\beta_B-1)|B_0|^2=\beta_B(\epsilon-\epsilon_c^T)-(\epsilon-\epsilon_c^L)\ ,\\ &\tau_A\Omega_A=c_0(\epsilon-\epsilon_c^T)-c_2|A_0|^2-c_3\beta_A|B_0|^2\ ,\end{aligned} \tag{5.15}$$

leads to real values of $|A_0|^2$ and $|B_0|^2$ for $\epsilon\geq\max(\epsilon_{\rm TR}^L,\epsilon_{\rm LR}^T)$. However, by examining the stability we find that one of the eigenvalues always has a positive real part. For example, perturbations with $\alpha=0$ have the growth rate

$$\begin{aligned}\tau_A\sigma_r=&-(|A_0|^2+|B_0|^2)\\ &+[(|A_0|^2+|B_0|^2)^2+(\beta_A\beta_B-1)|A_0|^2|B_0|^2]^{1/2}\ .\end{aligned} \tag{5.16}$$

Since the derivation of the coefficients has shown that $\beta_A\beta_B>1$ the "mixed" pattern (5.15), consisting of uniform TR and LR at the same location, is predicted to be unstable. This result also explains why the numerical simulations of Brand, Deissler, and Ahlers [13] did not show uniform coexisting solutions for $\beta_A\beta_B=1.125$, but they did for $\beta_A\beta_B=0.7$.

The next section presents some characteristic computer runs with the coupled Ginzburg-Landau equations. On the basis of our analytical discussion we expect uniform solutions of either TR or LR. Coexisting "mixed" states with nonzero amplitudes of TR and LR at the *same location* are expected—if at all—only for short-time intervals or over small distances.

VI. NUMERICAL SIMULATIONS

In this section we describe the results of two representative computer simulations with the coupled Ginzburg-Landau equations (4.10). To integrate the partial differential equations we use a finite difference Crank-Nicholson scheme with a spatial grid size of $\Delta x=0.25$ and a time resolution of $\Delta t=0.1$. The length of the channel is imposed to be 100. The stabilizing influence of sidewalls, which favors TR to occur at small Re, is considered by taking the *ad hoc* stability boundaries ϵ_c^T and ϵ_c^L shown in Fig. 2. These values give a codimension two point at $\mathrm{Re}^*\cong0.5$ in accordance with the experiment [8]. In order to guarantee *permanent* convection in the *convectively unstable* parameter region it is necessary to provide small but persistent inlet perturbations (reflecting entrance turbulence or other experimental noise) [23,25]. Since we do not perform any statistical evaluation of our numerical results we simply impose—instead of taking

noise—the following temporally constant inlet boundary conditions

$$A=0.001(\epsilon-\epsilon_c^T)^{1/2}\ ,\quad B=0.001(\epsilon-\epsilon_c^L)^{1/2}\ . \tag{6.1}$$

These values correspond to 0.1% of the respective saturation amplitudes. We emphasize that there is no information available about the actual experimental noise level in Ref. [8]. Moreover, it is not even clear that the inlet perturbations for A and B should be of the same order of magnitude. The values taken in (6.1) are therefore to be regarded as a first guess. Control runs with ten times smaller or greater inlet amplitudes gave quantitative modifications in the convectively unstable parameter region (e.g., displacement of a TR-LR transition) but no qualitative changes of the dynamics occurred. This is also in accordance with the prediction that the noise strength enters with the logarithm of its intensity [13,23,25]. For absolutely unstable parameters the system is insensitive to small external disturbances [13,14]. The remaining boundary conditions are

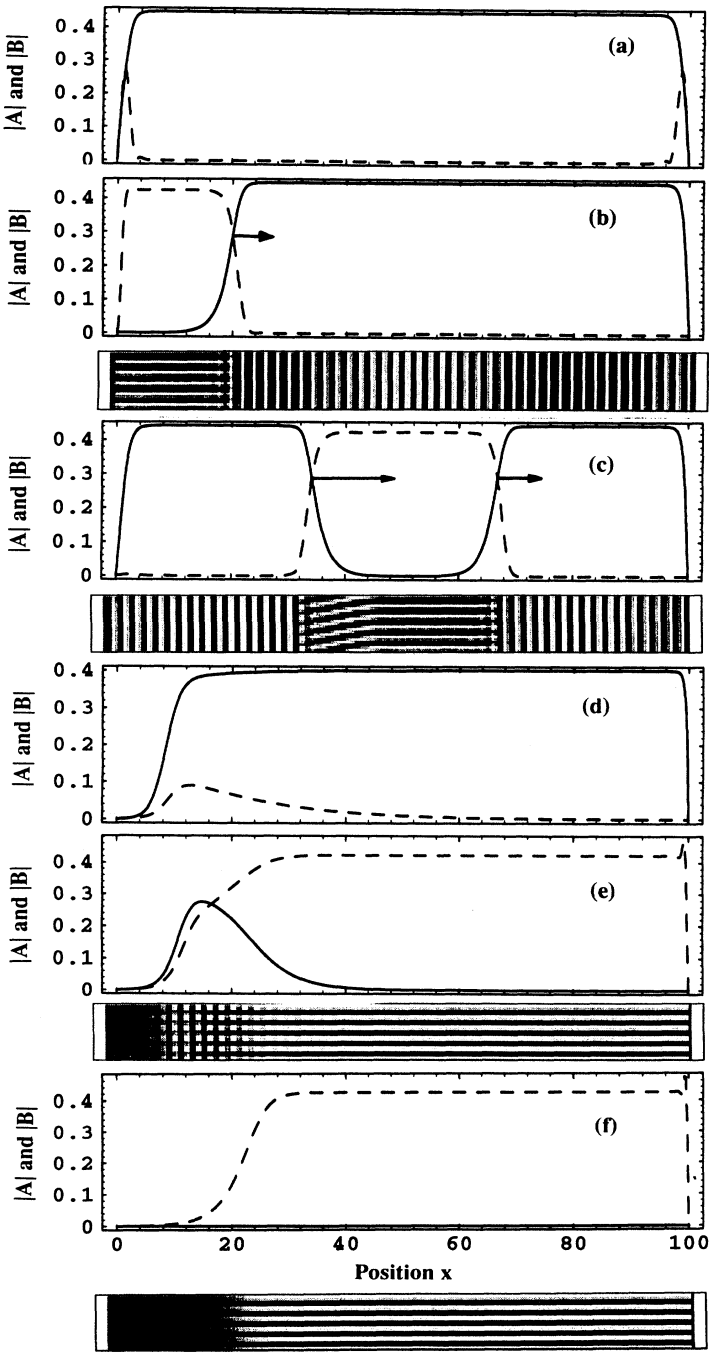

FIG. 3. Envelope $|A|$ for TR (solid line) and $|B|$ for LR (dashed) as a function of the streamwise coordinate x. The Rayleigh number is kept constant at $\epsilon=0.2$; the flow rate Re increases from (a) to (f). In some cases the two-dimensional density plots of the corresponding convection patterns (top view) are also given. (a) Stationary state of traveling TR with small LR contributions at the cell apertures at Re=0. (b) Transient state at Re=0.1. The front of a LR pattern invades in the downstream direction (see arrow) into the TR state. (c) Transient state at Re=0.25. A new TR front develops near the inlet and travels downstream. The leading LR front [same as in (b)] has not yet reached the outlet. The trailing TR front travels faster than the leading LR front (see arrows). (d) Re=0.75, stationary state of traveling TR close below ϵ_{LR}^T, the transition to LR. A small contribution from the LR pattern is already visible. (e) Re=0.82, stationary LR state close above this transition. The small remaining TR contribution dies out when the flow rate is increased further on. (f) Pure stationary LR pattern at Re=1.5. The distance from the inlet over which the envelope saturates increases with Re. The patterns of (d)–(f) exist in the convectively unstable parameter region (c.f. Fig. 2) since they are sustained by the inlet forcing (6.1).

$$A=B=0 \quad \text{(at outlet)}, \qquad \partial_x B=0 \quad \text{(at inlet and outlet)} \tag{6.2}$$

(recall that the amplitude equation for B is of fourth degree).

The first numerical experiment is a careful increase of the flow rate Re keeping $\epsilon=0.2$ constant. At the beginning of the run the envelopes A and B have been initialized by small random numbers. For Re=0 the linear temporal growth rate of A overwhelms that of B $[(\epsilon-\epsilon_c^T)/\tau_A > (\epsilon-\epsilon_c^L)/\tau_B]$, so that the TR mode wins the competition and the system saturates in an extended traveling TR state [Fig. 3(a)]. This state remains stable until Re≅0.07, which is in agreement with the experimental finding that TR patterns appear close to the ϵ axis (see Fig. 18 of Ref. [8]: region II). For Re slightly greater than 0.07 the front of a LR pattern invades at the channel inlet and propagates downstream into the TR state [Fig. 3(b)]. Increasing Re accelerates the front velocity, redecreasing slows it down again. For a Reynolds number below 0.07 the front propagates upstream. By carefully adjusting Re close to this transition value the front stops at its momentary position and TR and LR coexist in different areas of the convection cell. For $0.07<\mathrm{Re}<0.25$ the final state is achieved when the LR front has reached the outlet and the former traveling TR pattern is substituted by a stationary LR structure.

This LR pattern in turn becomes unstable above Re≅0.25 by a traveling TR structure whose front invades at the entrance of the cell. Figure 3(c) shows a situation where this TR front is already entering at the inlet before the aforementioned LR front has reached the outlet. Both leading and trailing fronts are propagating downstream with different velocities as indicated by the arrows. The resulting long-time structure is a homogeneous traveling TR pattern as for $\mathrm{Re}<0.07$.

The experiments of Ouazzani, Platten, and Mojtabi [8] did not show TR-LR transitions near Re≅0.07 and Re≅0.25; there the TR pattern persisted until Re≅0.8 and a crossover to LR appeared only above this value (c.f. Fig. 18 of Ref. [8]: transition from region IV to III). Upon increasing Re beyond ≅0.8 in our simulations we observe a third transition from TR to LR in a narrow Re interval close to ϵ_{LR}^T [Figs. 3(d) and 3(e)]. This threshold corresponds to the analytically predicted TR-LR transition at ϵ_{LR}^T (see Sec. V and Fig. 2), where an extended TR state becomes unstable against LR perturbations. The exact location of this transition in the ϵ-Re control parameter plane slightly depends on the strength of the inlet forcing (6.1). By ramping Re back and forth we verified this crossover to be free of a hysteresis as in the experiment [8]. The time dependence of the vertical velocity field w (at $x=40$, say) belonging to the envelopes shown in Fig. 3(e) consists of a strong DC signal (from the stationary LR pattern) superimposed by a small AC offset from the weak traveling TR contribution. The similarity to the experimental laser Doppler signal of Ref. [8] (see their Fig. 7) is striking. Note that the model of Brand, Deissler, and Ahlers [13] predicts this transition to appear close to their ϵ_5, which corresponds to our ϵ_{TR}^L. This difference arises since they used a coupling coefficient $\beta_A=0.75$ being smaller than unity.

Figure 3(f) shows that the TR contribution totally dies out when the flow rate is increased further on. Simultaneously the saturated LR pattern is pushed more and more out of the container. The structures shown in Figs. 3(d)–3(f) exist in spite of the *convectively* unstable parameter conditions ($\epsilon<\epsilon_{\mathrm{abs}}^{T,L}$). They are sustained by the finite entrance forcing (6.1) [23,25] since they die out as soon as (6.1) is replaced by a homogeneous boundary condition.

In the second simulation run we vary ϵ at the fixed through-flow rate Re=0.1 to test the theoretically predicted LR-TR transition at ϵ_{TR}^L (c.f. Fig. 2). Starting from the fully developed stationary LR state at $\epsilon=0.2$ and Re=0.1 [Fig. 4(a)] we suddenly decrease ϵ to 0.08, i.e., below the threshold $\epsilon_{\mathrm{TR}}^L(\mathrm{Re}=0.1)\cong 0.1$. As can be seen from Fig. 4(b), a TR front develops in the entrance region and invades into the LR state. By returning to $\epsilon=0.2$ one obtains a new LR front [Fig. 4(c)]. In contrast to the situation presented in Fig. 3(c) the slower LR front now follows the faster TR front. As before, accurate adjustment of the Rayleigh number close to ϵ_{TR}^L brings the trailing front to a halt or makes it propagating in the upstream direction for $\epsilon<\epsilon_{\mathrm{TR}}^L$. This transition, showing no hysteresis in our simulations, is not in complete accordance with the experiment [8]. There, a crossover from TR to LR by increasing ϵ has also been observed, but the corresponding back transition was not. Brand, Deissler, and Ahlers [13] do not predict any non-

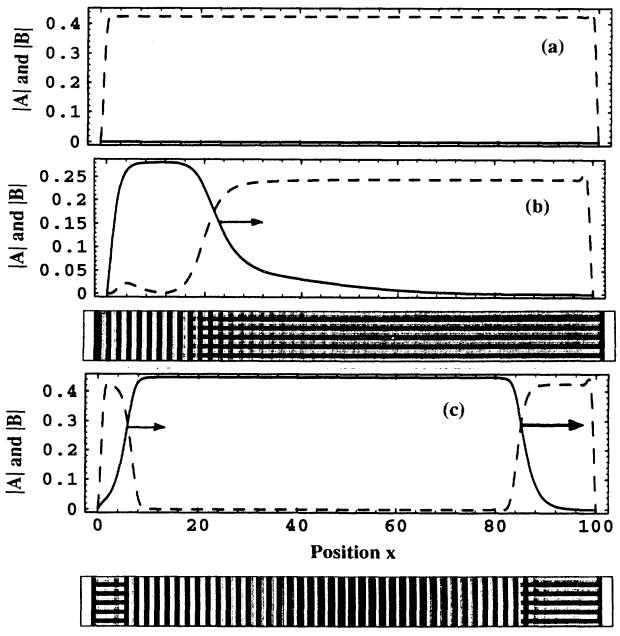

FIG. 4. Same as Fig. 3 but for fixed flow rate Re=0.1 and for different Rayleigh numbers ϵ. (a) Stationary LR state at $\epsilon=0.2$. (b) Transient state at $\epsilon=0.08$. Since $\epsilon<\epsilon_{\mathrm{TR}}^L\cong 0.1$ the LR state is unstable and a TR front invades (see arrow). (c) Transient state at $\epsilon=0.2$. After the reincrease back to $\epsilon=0.2$ a new LR front appears near the inlet. The leading TR front [same as in (b)] has not yet reached the outlet. Propagation velocities and directions are indicated by the arrows.

linear transition at all in the region $\mathrm{Re}<\mathrm{Re}^*$. On increasing ϵ they observe stable TR up to $\epsilon=1$.

VII. SUMMARY

In the present article we derive the coupled envelope equations for travelling transverse (TR) and stationary longitudinal roll (LR) patterns in Rayleigh-Bénard convection with a horizontal flow. Fit formulas of the coefficients are given for Reynolds numbers up to unity and a Prandtl number of 5.8. The calculations are performed for an idealized convection cell with rigid top and bottom plates but free-slip sidewalls. The tendency of the lateral boundaries to stabilize TR at weak flow rates is incorporated into the model by taking *ad hoc* stability boundaries. The competitive nonlinear dynamics between TR and LR strongly depends on the numerical values of the coupling coefficients β_A and β_B. The values $\beta_A\cong\beta_B\cong 1.25$ we find are reasonably far apart from those where a qualitative change in the dynamics appears, i.e., $\beta_A\beta_B<1$ [see Eq. (5.16)]. Nevertheless, we cannot exclude that a rigorous treatment of the sidewall boundary condition would have led to a qualitative different model.

In our model coexisting states with nonzero amplitudes of TR and LR at the same location appear as unstable solutions of the amplitude equations. The experimentally observed transition from the extended TR state to the LR pattern by increasing the flow rate has been analytically calculated and numerically confirmed. Additional TR-LR transitions and solutions with propagating fronts between the two structures have been found in our simulations but not reported in the experiments [8]. This might be due to the experimental laser Doppler velocimetry which only allows *local* measurements but gives no hint about the *global* convective structure. Very slow transients (e.g., slowly traveling fronts) therefore might eventually appear as stationary states. Further experimental work with a flow visualization of the entire convection cell [9] is necessary to have a better test of the theoretical predictions.

ACKNOWLEDGMENTS

We wish to express our gratitude to Professor Guenter Ahlers for stimulating discussions. We also acknowledge contributions from E. Bodenschatz, K. L. Babcock, and M. Lücke. H.M.W. and M.T. thank the Center for Nonlinear Sciences of the University of California, Santa Barbara, for hospitality. This work is supported by Deutsche Forschungsgemeinschaft, Royal Norwegian Council for Scientific and Industrial Research, and the National Science Foundation under Grant No. NSF-DMR91-17428.

APPENDIX

The 8×8 matrix operator in Eq. (4.1) is defined by

$$\underline{L}=\begin{bmatrix} \partial_z & 0 & 0 & 0 & -1 & 0 & 0 & 0 \\ 0 & \partial_z & 0 & 0 & 0 & -1 & 0 & 0 \\ \partial_x & \partial_y & \partial_z & 0 & 0 & 0 & 0 & 0 \\ 0 & 0 & 0 & \partial_z & 0 & 0 & 0 & -1 \\ d_1 & 0 & -\mathrm{Re}U' & 0 & \partial_z & 0 & -\partial_x & 0 \\ 0 & d_1 & 0 & 0 & 0 & \partial_z & -\partial_y & 0 \\ 0 & 0 & -d_1 & -\mathrm{Ra} & \partial_x & \partial_y & \partial_z & 0 \\ 0 & 0 & 1 & d_2 & 0 & 0 & 0 & \partial_z \end{bmatrix}, \tag{A1}$$

where

$$d_1=\partial_x^2+\partial_y^2-\mathrm{Re}U\partial_x-\frac{1}{\sigma}\partial_t\ ,$$
$$d_2=\partial_x^2+\partial_y^2-\sigma\,\mathrm{Re}U\partial_x-\partial_t\ . \tag{A2}$$

The expansion of $\underline{L}$ in powers of $\delta^{1/2}$ is found by inserting the multiple scale expansions for ∂_x and ∂_t and $\mathrm{Ra}=\mathrm{Ra}_c^{L,T}+\mathrm{Ra}_{c0}(\epsilon-\epsilon_c^{L,T})$, where the term in parentheses is of order δ^2:

$$\underline{L}_0=\underline{L}\,|_{\mathrm{Ra}=\mathrm{Ra}_c^{L,T}}\ ,$$
$$\underline{L}_{1/2}=\underline{H}\partial_{T1/2}+\underline{D}\partial_{X1/2}\ ,$$
$$\underline{L}_1=\underline{H}\partial_{T1}+\underline{D}\partial_{X1}+\underline{E}\partial_{X1/2}^2\ , \tag{A3}$$
$$\underline{L}_{3/2}=\underline{H}\partial_{T3/2}+\underline{D}\partial_{X3/2}+2\underline{E}\partial_{X1/2}\partial_{X1}\ ,$$
$$\underline{L}_2=\underline{H}\partial_{T2}+\underline{D}\partial_{X2}+\underline{E}(\partial_{T1}^2+2\partial_{X1/2}\partial_{X3/2})+\mathrm{Ra}_{c0}\frac{\epsilon-\epsilon_c^{L,T}}{\delta^2}\underline{F}\ .$$

Here, $\underline{H}$, $\underline{D}$, $\underline{E}$, and $\underline{F}$ denote sparse 8×8 matrices. Their nonzero elements are

$$H_{51}=H_{62}=-H_{73}=-1/\sigma\ ,\quad H_{84}=-1\ ,$$
$$D_{51}=D_{62}=-D_{73}=2\partial_x-\mathrm{Re}U\ ,\quad D_{84}=2\partial_x-\sigma\,\mathrm{Re}U\ ,$$
$$D_{31}=-D_{57}=D_{75}=1\ , \tag{A4}$$
$$E_{51}=E_{62}=-E_{73}=E_{84}=1\ ,$$
$$F_{74}=-1\ .$$

In expanding the nonlinearity $N(\varphi,\varphi)=(1/\sigma)(\mathbf{v}\cdot\nabla)(0,0,0,0,u,v,-w,\sigma\theta)^t$ (the first argument φ refers to $\mathbf{v}$ and the second to the transposed vector) one obtains with (4.3b) and (4.4),

$$N_2=N(\varphi_1,\varphi_1)\ ,$$
$$N_{3/2}=N(\varphi_1,\varphi_{3/2})+N(\varphi_{3/2},\varphi_1)+(\mathrm{NDT})\ , \tag{A5}$$
$$N_3=N(\varphi_1,\varphi_2)+N(\varphi_{3/2},\varphi_{3/2})+N(\varphi_2,\varphi_1)+(\mathrm{NDT})\ .$$

Here NDT stands for nonlinear derivative terms with respect to the slow spatial scales $X_{1/2}$ and/or X_1. Up to $O(\delta^3)$ these terms do not contribute to the amplitude equation because their x and y dependencies are not in resonances with the adjoint solutions.

[1] R. A. Brown, *Analytical Methods in Planetary Boundary-Layer Modelling* (Hilger, London, 1974).

[2] For a review, see R. E. Kelly, in *Proceedings of the International Conference on Physical Chemistry and Hydrodynamics,* edited by D. B. Spalding (Advance Publ., London, 1977), p. 65.

[3] P. Huerre, in *Propagation in Systems Far from Equilibrium,* edited by J. E. Wesfreid, H. R. Brand, P. Manneville, G. Albinet, and N. Boccara (Springer, Berlin, 1988); in *Instabilities and Nonequilibrium Structures,* edited by E. Tirapegui and D. Villarroel (Reidel, Dordrecht, 1987).

[4] J. M. Luijkx and J. K. Platten, Int. J. Heat Mass Transfer **24**, 1287 (1981).

[5] K. C. Chiu and F. Rosenberger, Int. J. Heat Mass Transfer **30**, 1645 (1987); see also references cited therein.

[6] A. Pocheau, V. Croquette, P. Le Gal, and C. Poitou, Europhys. Lett. **3**, 915 (1987).

[7] M. T. Ouazzani, J. P. Caltagirone, G. Meyer, and A. Mojtabi, Int. J. Heat Mass Transfer **32**, 261 (1989).

[8] M. T. Ouazzani, J. K. Platten, and A. Mojtabi, Int. J. Heat Mass Transfer **33**, 1417 (1990), and (unpublished).

[9] S. Trainoff, G. Ahlers, and D. S. Cannel (private communication).

[10] K. S. Gage and W. H. Reid, J. Fluid Mech. **33**, 21 (1968).

[11] M. Tveitereid, Z. Angew. Math. Mech. (ZAMM) **54**, 533 (1974).

[12] J. M. Luijkx, Ph.D. thesis, University of Mons (Belgium), 1983.

[13] H. R. Brand, R. J. Deissler, and G. Ahlers, Phys. Rev. A **43**, 4262 (1991). To facilitate a comparison with our results we provide a list of the coefficients translating from their notation into ours: $\tau_0^{T,L}\rightarrow\tau_{A,B}$; $v^{T,L}\rightarrow v_{A,B}$; $\chi^{T,L}\rightarrow\epsilon-\epsilon_c^{T,L}$; $\gamma^{T,L}\rightarrow\xi^2_{A,B}$; $\beta^{T,L}\rightarrow 1$; $\delta^{T,L}\rightarrow\beta_{A,B}$; $\epsilon_1\rightarrow\epsilon_c^L$; $\epsilon_3\rightarrow\epsilon_c^T$; $\epsilon_4\rightarrow\epsilon_{\rm abs}^T$; $\epsilon_5\rightarrow\epsilon_{\rm TR}^T$; $\epsilon_7\rightarrow\epsilon_{\rm LR}^T$.

[14] H. W. Müller, M. Lücke, and M. Kamps, Europhys. Lett. **10**, 451 (1989); Phys. Rev. A **45**, 3714 (1992); in *Ordered and Turbulent Patterns in Taylor-Couette Flow,* Vol. 297 of *NATO Advanced Science Institute, Series B: Physics,* edited by C. D. Andereck and F. Hayout (Plenum, New York, 1992).

[15] P. G. Drazin and W. H. Reid, *Hydrodynamic Stability* (Cambridge, University Press, Cambridge, England, 1981).

[16] See, e.g., S. Chandrasekhar, *Hydrodynamic and Hydromagnetic Stability* (Oxford University Press, New York, 1961).

[17] H. B. Squire, Proc. R. Soc. London Ser. A **142**, 621 (1933).

[18] A. Schlüter, D. Lortz, and F. Busse, J. Fluid Mech. **23**, 129 (1965).

[19] L. A. Segel, J. Fluid Mech. **38**, 203 (1969).

[20] A. C. Newell and J. A. Whitehead, J. Fluid Mech. **38**, 279 (1969).

[21] C. M. Bender and S. A. Orszag, *Advanced Methods for Scientists and Engineers* (McGraw-Hill, New York, 1978).

[22] D. R. Jenkins and M. R. E. Proctor, J. Fluid Mech. **139**, 461 (1984); D. R. Jenkins, *ibid.* **178**, 491 (1987).

[23] R. J. Deissler, J. Stat. Phys. **40**, 371 (1985).

[24] M. Tveitereid and H. W. Müller (unpublished). The saddle points in the complex wave-number plane are approximately $k_s=(iv_B\tau_B/4\lambda_B)^{1/3}$. The corrections to k_s from ∂_x^2 and ∂_x^3 are both less than 1% for $\mathrm{Re}\leq 1$.

[25] R. J. Deissler, Physica D **25**, 233 (1987); J. Stat. Phys. **54**, 1459 (1989).

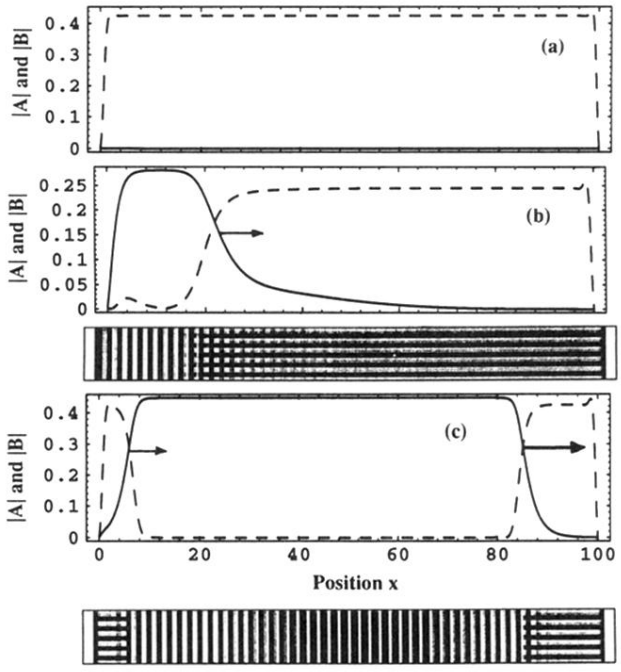

FIG. 4. Same as Fig. 3 but for fixed flow rate Re$=0.1$ and for different Rayleigh numbers ϵ. (a) Stationary LR state at $\epsilon=0.2$. (b) Transient state at $\epsilon=0.08$. Since $\epsilon<\epsilon_{\mathrm{TR}}^{L}\cong 0.1$ the LR state is unstable and a TR front invades (see arrow). (c) Transient state at $\epsilon=0.2$. After the reincrease back to $\epsilon=0.2$ a new LR front appears near the inlet. The leading TR front [same as in (b)] has not yet reached the outlet. Propagation velocities and directions are indicated by the arrows.